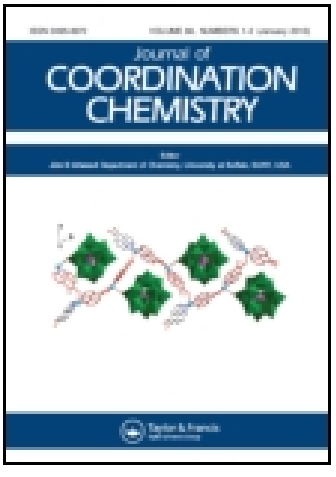

Journal of Coordination Chemistry
Publication details, including instructions for authors and subscription information:
http://www.tandfonline.com/loi/gcoo20

Two independent, 1-D metal-organic nanotubes based on rings or helical chain units

Xia Zhu[a], Shan Zhao[a], Yan-Fen Peng[a], Bao-Long Li[a] & Hai-Yan Li[a]
[a] Key Laboratory of Organic Synthesis of Jiangsu Province, College of Chemistry, Chemical Engineering and Materials Science, Soochow University, Suzhou, P.R. China

Accepted author version posted online: 16 Apr 2014.Published online: 12 May 2014.

Journal of Coordination Chemistry, 2014
Vol. 67, No. 8, 1317–1331, http://dx.doi.org/10.1080/00958972.2014.915523

Two independent, 1-D metal–organic nanotubes based on rings or helical chain units

XIA ZHU, SHAN ZHAO, YAN-FEN PENG, BAO-LONG LI* and HAI-YAN LI

Key Laboratory of Organic Synthesis of Jiangsu Province, College of Chemistry, Chemical Engineering and Materials Science, Soochow University, Suzhou, P.R. China

(*Received 31 August 2013; accepted 26 February 2014*)

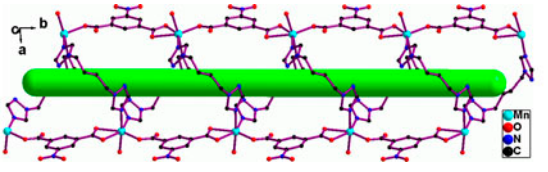

Three coordination polymers $\{[Mn(bte)(NO_2\text{-}1,3\text{-}bdc)(H_2O)]\cdot H_2O\}_n$ (**1**), $\{[Mn(btp)(NO_2\text{-}1,3\text{-}bdc)(H_2O)]\cdot 2H_2O\}_n$ (**2**), and $\{[Mn(btb)(NO_2\text{-}1,3\text{-}bdc)(H_2O)]\cdot H_2O\}_n$ (**3**) (bte, 1,2-bis(1,2,4-triazol-1-yl) ethane; btp, 1,3-bis(1,2,4-triazol-1-yl)propane; btb, 1,4-bis(1,2,4-triazol-1-yl)butane, NO_2-1,3-H_2bdc, 5-nitroisophthalic acid) were synthesized by combination of bte, btp, and btb, conformationally flexible ligands with different spacer lengths, and the rigid $[NO_2\text{-}1,3\text{-}bdc]^{2-}$. In **1**, two $[NO_2\text{-}1,3\text{-}bdc]^{2-}$ anions link adjacent $[Mn_2(bte)_2]$ rings to give an independent, 1-D metal–organic nanotube (MONT). The structure of **2** is an undulating 2-D (4,4) network. In **3**, the combination of a $[Mn(btb)]_n$ single helical chain and two $[Mn(NO_2\text{-}1,3\text{-}bdc)]_n$ linear chains assemble an intriguing independent, 1-D MONT. An interesting structural feature of **1** and **3** is that the nitro groups of each 1-D MONT interpenetrate into two adjacent 1-D MONTs to form a 1-D → 2-D interdigitated array. 3-D architectures in **1** and **3** are assembled *via* hydrogen bond interactions. The luminescent properties and thermal stabilities of **1**, **2**, and **3** were investigated.

Keywords: Metal–organic nanotube; Coordination polymer; Manganese complex; Interdigitated array; Luminescence

1. Introduction

Since the first discovery of carbon nanotubes (CNTs) [1], the design and synthesis of metal–organic nanotubes (MONTs) have attracted intensive interest due to topological structures and potential applications in gas storage, ion exchange, catalysis, and sensor technologies [2–15]. Unlike CNTs, MONTs are constructed by organic ligands and metal ions. In order to assemble 1-D MONTs, the linking mode of the ligand should fit the coordination geometry of the metal ion. An effective strategy is to generate a ring or

*Corresponding author. Email: libaolong@suda.edu.cn

cyclic subunit *via* connection of a metal ion by an organic ligand, and then utilize a second organic ligand to link the ring subunits into a 1-D MONT. Although many metal–organic porous frameworks have been synthesized, only a limited number of MONTs have been reported [2–15].

Contrary to rigid spacers, flexible ligands that can adopt different conformations according to the geometric needs of the different metal ions may produce coordination polymers with novel topologies [16–19]. The three flexible bis(triazole) ligands, 1,2-bis(1,2,4-triazol-1-yl)ethane (bte) [20], 1,3-bis(1,2,4-triazol-1-yl)propane (btp) [21], and 1,4-bis(1,2,4-triazol-1-yl)butane (btb) [22], have different alkane spacer lengths and conformational flexibilities from the relative orientations of the CH_2 groups; they have proven to be good bridging ligands for construction of metal–organic frameworks. For example, $\{[Zn(btp)(1,4\text{-bdc})][Zn(btp)(1,4\text{-bdc})_{0.5}Cl]\cdot H_2O\}_n$ (1,4-H_2bdc = 1,4-benzenedicarboxylic acid) displays a new type of entanglement in that only a half of the loops of the 2-D network are polythreaded by 1-D chains containing alternating rings and rods [21].

Because of the diversity of the coordination modes and high structural stability, carboxylate ligands are frequently used for construction of MOFs [23, 24]. The combination of different spacer lengths and conformational flexibilities of the bis(triazole) ligands and the rigid 5-nitroisophthalate [$(NO_2\text{-}1,3\text{-bdc})^{2-}$] with an angle of ca. 120° between two carboxylate groups can construct intriguing topologies [25–27].

In order to investigate the influence of the spacer lengths and conformational flexibilities of the ligands on the supramolecular architectures and to construct new topologies, in the present work, we synthesized three coordination polymers $\{[Mn(bte)(NO_2\text{-}1,3\text{-bdc})(H_2O)]\cdot H_2O\}_n$ (**1**), $\{[Mn(btp)(NO_2\text{-}1,3\text{-bdc})(H_2O)]\cdot 2H_2O\}_n$ (**2**), and $\{[Mn(btb)(NO_2\text{-}1,3\text{-bdc})(H_2O)]\cdot H_2O\}_n$ (**3**) by combination of bte, btp, btb, and NO_2-1,3-H_2bdc. The syntheses, structures, luminescence properties, and thermal stabilities of **1–3** are presented.

2. Experimental

2.1. *Materials and general methods*

All reagents were of analytical grade and used without purification. The linkers bte, btp, and btb were synthesized according to literature methods [28]. C, H, and N elemental analyses were performed on a Perkin–Elmer 240C analyser. IR spectra were obtained as KBr pellets on a Nicolet 170SX FT-IR spectrophotometer from 4000 to 400 cm^{-1}. PXRD data were collected at room temperature on a D/MAX-3C diffractometer with CuKα radiation (λ = 1.5406 Å). The luminescence measurements were carried out in the solid state at room temperature with a Perkin–Elmer LS50B spectrofluorimeter. TGA was carried out using a Thermal Analyst 2100 TA Instrument and SDT 2960 Simultaneous TGA-DTA Instrument in flowing dinitrogen at a heating rate of 10 °C min^{-1}.

2.2. *Synthesis of $\{[Mn(bte)(NO_2\text{-}1,3\text{-bdc})(H_2O)]\cdot H_2O\}_n$ (1)*

A solution of NO_2-1,3-H_2bdc (0.2 mM) in 10 mL H_2O was adjusted to approximately pH 6.5 with 0.38 mL of a 1.0 M NaOH solution. Then bte (0.2 mM) in 10 mL CH_3OH was added. This solution was added to one arm of an "H-shaped" tube, and Mn

$(NO_3)_2{\cdot}6H_2O$ (0.2 mM) in 20 mL water was added to the other arm of the tube. Colorless, block-shaped crystals of **1** (0.054 g, 58% yield) were obtained after one month at room temperature. Anal. Calcd for $C_{14}H_{15}MnN_7O_8$: C, 36.22; H, 3.26; N, 21.12%. Found: C, 36.19; H, 3.22; N, 21.05. IR data (cm^{-1}): 3634m, 3418m, 1624s, 1558s, 1539s, 1458m, 1393m, 1365s, 1281s, 1254w, 1211w, 1138m, 1096w, 1011w, 988m, 930w, 887m, 791m, 733s, 671m, 644w.

2.3. *Synthesis of {[Mn(btp)(NO_2-1,3-bdc)(H_2O)]·2H_2O}$_n$ (2)*

The synthetic procedure of **2** was similar to the synthesis of **1**, except that btp (0.20 mM) was used instead of bte. Colorless, block-shaped crystals of **2** (0.061 g, 61% yield) were obtained after three weeks at room temperature. Anal. Calcd for $C_{15}H_{19}MnN_7O_9$: C, 36.30; H, 3.86; N, 19.76%. Found: C, 36.23; H, 3.82; N, 19.71. IR data (cm^{-1}): 3742s, 3680 m, 1694w, 1647w, 1516s, 1481m, 1427m, 1396m, 1369m, 1342w, 1285w, 1130w, 1072w, 988w, 945w, 894w, 779s, 732s, 675s, 586w, 497w.

2.4. *Synthesis of {[Mn(btb)(NO_2-1,3-bdc)(H_2O)]·H_2O}$_n$ (3)*

The synthetic procedure of **3** was similar to the synthesis of **1**, except that btb (0.20 mM) was used instead of bte. Colorless, prismatic crystals of **3** (0.070 g, 71% yield) were obtained after one month at room temperature. Anal. Calcd for $C_{16}H_{19}MnN_7O_8$ (**3**): C, 39.03; H, 3.89; N, 19.92%. Found: C, 38.96; H, 3.85; N, 19.86. IR data (cm^{-1}): 3420s, 3247s, 3146s, 1628s, 1563s, 1534s, 1452w, 1368m, 1342m, 1281m, 1206w, 1136s, 1099w, 1074w, 1024w, 987s, 928w, 884m, 790w, 735s, 674m, 651w, 513w.

Table 1. Crystallographic data and structural refinement parameters for **1**, **2,** and **3**.

	1	**2**	**3**
Formula	$C_{14}H_{15}MnN_7O_8$	$C_{15}H_{19}MnN_7O_9$	$C_{16}H_{19}MnN_7O_8$
Fw	464.27	496.31	492.32
Crystal system	Monoclinic	Triclinic	Monoclinic
Space group	*C2/c*	$P\bar{1}$	$P2_1/n$
Temp (K)	293(2)	293(2)	223(2)
a (Å)	20.658(3)	10.123(2)	11.3966(18)
b (Å)	10.2720(7)	10.2447(13)	10.2604(15)
c (Å)	20.690(3)	11.051(3)	17.864(3)
α (°)	90	70.70(3)	90
β (°)	122.443(15)	80.89(3)	94.538(4)
γ (°)	90	68.36(3)	90
V (Å^3)	3705.2(9)	1004.6(4)	2082.3(6)
Z	8	2	4
ρ_{Calcd} (g/cm^3)	1.665	1.641	1.570
μ (mm^{-1})	0.775	0.723	0.694
F (0 0 0)	1896	510	1012
Reflections collected	17199	9786	11626
Unique reflections	3367 [*R*(int) = 0.0462]	3646 [*R*(int) = 0.0419]	4736 [*R*(int) = 0.0323]
Parameters	283	309	305
Goodness of fit	1.069	1.075	1.078
R_1 [$I > 2\sigma(I)$]	0.0526	0.0539	0.0492
wR_2 (all data)	0.1290	0.1316	0.1059

Table 2. Selected bond lengths [Å] and angles [°] for **1**, **2,** and **3**.

1			
Mn(1)–N(3)	2.258(3)	Mn(1)–N(6A)	2.215(3)
Mn(1)–O(1)	2.139(2)	Mn(1)–O(3B)	2.344(2)
Mn(1)–O(4B)	2.264(2)	Mn(1)–O(7)	2.176(3)
N(6A)–Mn(1)–N(3)	93.65(11)	O(1)–Mn(1)–N(3)	89.14(10)
N(3)–Mn(1)–O(3B)	88.29(10)	N(3)–Mn(1)–O(4B)	86.08(10)
O(7)–Mn(1)–N(3)	175.36(10)	O(1)–Mn(1)–N(6A)	126.31(10)
N(6A)–Mn(1)–O(3B)	84.01(9)	N(6A)–Mn(1)–O(4B)	140.65(9)
O(7)–Mn(1)–N(6A)	90.70(10)	O(1)–Mn(1)–O(3B)	149.68(9)
O(1)–Mn(1)–O(4B)	93.03(9)	O(1)–Mn(1)–O(7)	86.98(10)
O(4B)–Mn(1)–O(3B)	56.65(8)	O(7)–Mn(1)–O(3B)	93.78(9)
O(7)–Mn(1)–O(4B)	91.59(10)		
2			
Mn(1)–N(3)	2.240(3)	Mn(1)–N(6B)	2.219(3)
Mn(1)–O(1)	2.267(3)	Mn(1)–O(2)	2.385(2)
Mn(1)–O(3A)	2.117(3)	Mn(1)–O(7)	2.177(3)
N(6B)–Mn(1)–N(3)	93.96(11)	O(1)–Mn(1)–N(3)	86.81(10)
O(2)–Mn(1)–N(3)	94.20(10)	O(3A)–Mn(1)–N(3)	89.73(11)
O(7)–Mn(1)–N(3)	173.83(11)	O(1)–Mn(1)–N(6B)	137.71(10)
O(2)–Mn(1)–N(6B)	81.64(10)	O(3A)–Mn(1)–N(6B)	130.20(11)
O(7)–Mn(1)–N(6B)	90.83(11)	O(1)–Mn(1)–O(2)	56.19(9)
O(3[a])–Mn(1)–O(1)	92.05(10)	O(7)–Mn(1)–O(1)	92.26(11)
O(3[a])–Mn(1)–O(2)	147.61(10)	O(7)–Mn(1)–O(2)	90.34(11)
O(3[a])–Mn(1)–O(7)	84.20(11)		
3			
Mn(1)–N(3)	2.267(2)	Mn(1)–N(6A)	2.204(2)
Mn(1)–O(1)	2.1091(16)	Mn(1)–O(3B)	2.3343(16)
Mn(1)–O(4B)	2.2744(16)	Mn(1)–O(7)	2.1912(19)
N(6A)–Mn(1)–N(3)	89.05(8)	O(1)–Mn(1)–N(3)	89.06(7)
O(3B)–Mn(1)–N(3)	90.89(7)	O(4B)–Mn(1)–N(3)	86.20(7)
O(7)–Mn(1)–N(3)	174.32(7)	O(1)–Mn(1)–N(6A)	116.33(7)
O(3B)–Mn(1)–N(6A)	91.97(7)	O(4B)–Mn(1)–N(6A)	148.58(7)
O(7)–Mn(1)–N(6A)	91.42(8)	O(3B)–Mn(1)–O(1)	151.69(6)
O(4B)–Mn(1)–O(1)	94.65(6)	O(7)–Mn(1)–O(1)	95.80(7)
O(3B)–Mn(1)–O(4B)	57.12(5)	O(3B)–Mn(1)–O(7)	83.43(7)
O(4B)–Mn(1)–O(7)	90.46(7)		

Symmetry transformations used to generate equivalent atoms: for **1**, A, $-x+1/2$, $-y+1/2$, $-z$; B, x, $y+1$, z; for **2**, A, x, $y+1$, z; B, x, y, $z-1$; for **3**, A, x, $y+1$, z; B, x, y, $z-1$.

2.5. *X-ray crystallography*

Suitable single crystals of **1**, **2,** and **3** were carefully selected under an optical microscope and glued to thin glass fibers. The diffraction data were collected on Rigaku Mercury or Saturn CCD diffractometers with graphite-monochromated MoKα radiation. Intensities were collected by the ω scan technique. The structures were solved by direct methods and refined with full-matrix least-squares (SHELXTL-97) [29]. All non-hydrogen atoms were anisotropically refined. The positions of the hydrogens of bte, btp, btb, and $(NO_2\text{-}1,3\text{-bdc})^{2-}$ were generated geometrically, riding on their parent atoms with $U_{iso}(H) = 1.2U_{eq}(C)$. The hydrogens of waters were obtained from successive Fourier syntheses. The crystal data and structural refinement parameters of **1**, **2,** and **3** are given in table 1. Selected bond lengths and angles are given in table 2.

3. Results and discussion

3.1. *Crystal structures*

Compound **1** exhibits an independent, 1-D MONT framework based on ring units. The asymmetric unit contains one Mn(II), one $(NO_2\text{-}1,3\text{-bdc})^{2-}$, one bte, one coordinated water, and one lattice water. Each Mn(II) displays a distorted, $\{MnN_2O_4\}$ octahedral coordination geometry [figure 1(a)], coordinated by two triazole nitrogens from two bte ligands (Mn(1)–N(3), 2.258(3) Å; Mn(1)–N(6A), 2.215(3) Å), three carboxylate oxygens from two $[NO_2\text{-}1,3\text{-bdc}]^{2-}$ ligands (Mn(1)–O(1), 2.139(2) Å; Mn(1)–O(3B), 2.344(2) Å; Mn(1)–O(4B), 2.264(2) Å), and coordinated water (Mn(1)–O(7) 2.176(3) Å)). The short carboxylate Mn(1)–O(1) distance arises from a monodentate carboxylate, while the other two longer distances are from a chelating carboxylate. The Mn–N and Mn–O bond lengths are normal relative to other Mn(II) complexes [30–37]. Each bte has a *gauche*-conformation with a dihedral angle of 53.0° between the two triazole rings and a N(1)–C(1)–C(2)–N(4) torsion angle of 117.7(3)°. Each bte has bis-monodentate coordination and bridges two Mn(II) ions with a Mn···Mn separation of 7.6809(14) Å. Two bte ligands bridge two Mn(II) ions to form a $Mn_2(bte)_2$ 18-membered ring with a near-rhomboidal shape, with distances along the edges of 6.0 and 6.1 Å and across the diagonals of 7.7 and 9.4 Å [figure 1(b)].

Each $(NO_2\text{-}1,3\text{-bdc})^{2-}$ bridges two Mn(II) ions with a Mn···Mn separation of 10.2720(7) Å. Further, adjacent $[Mn_2(bte)_2]$ rings are linked by two $(NO_2\text{-}1,3\text{-bdc})^{2-}$ ligands to give a 1-D MONT framework. One of the simplest and most effective methods for the construction of an independent 1-D MONT, is the connection of ring or cyclic subunits by two chains, of which **1** is a good example.

Independent 1-D MONTs are quite scarce [7–15]. For example, Sun and coworkers reported an interesting 1-D MONT, $[Zn(ATIBDC)(bpy)]\cdot 3H_2O$ (bpy = 4,4′-bipyridine, H_2ATIBDC = 5-amino-2,4,6-triiodoisophthalic acid), in which the Zn(II) ion is first connected by bpy ligands to generate a $[Zn_4(bpy)_4]$ square as the subunit, and then, the second ligand $(ATIBDC)^{2-}$ links the squares from each of the four vertexes to generate a 1-D nanotubular framework [7, 8]. Dong and coworkers reported an Ag complex in which the Ag is

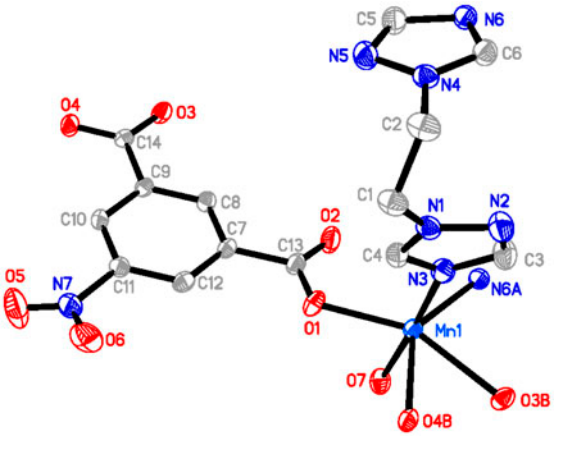

Figure 1(a). The coordination environment of Mn(II) in **1** shown with 50% probability thermal ellipsoids.

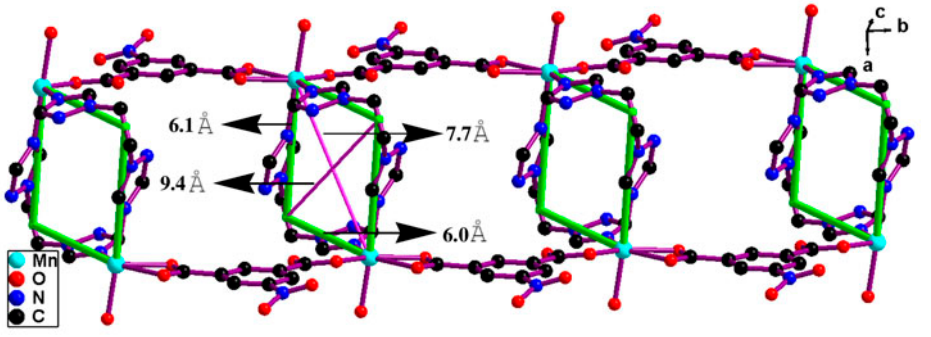

Figure 1(b). Perspective view of an independent, 1-D MONT for **1**.

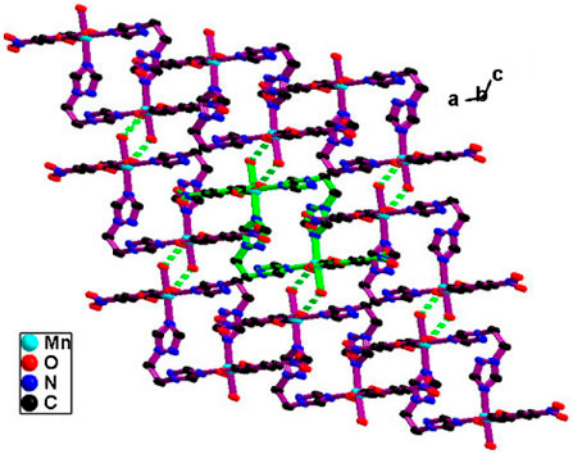

Figure 1(c). The 3-D hydrogen bond architecture in **1**. The bright green dashed lines exhibit the O(7)···O(3)^{i} hydrogen bond interaction.

a square planar, four-connecting node, and bent tetradentate ligands connect the Ag ions to generate a 1-D tube motif [9]. Sun and coworkers synthesized [Zn(TITMB)(OAc)(OH)]·8.5H_2O (TITMB = 1,3,5-tris(imidazol-1-ylmethyl)-2,4,6trimethylbenzene), in which four zinc(II) ions and two of the three pendant arms from four TITMB ligands form a 48-membered macrocyclic ring, and the macrocyclic rings are then connected by Zn–N coordination bonds to give an infinite, 1-D tube-like chain [10]. Luo and coworkers synthesized $[Cd_3(BPT)_2(phen)_3(H_2O)]_4 \cdot 5H_2O$ (H_3BPT = biphenyl-3,4′,5tricarboxylic acid, phen = 1,10-phenanthroline), in which the two types of SBUs, $[Cd_2(CO_2)_4(phen)_4]$ and [Cd$(CO_2)_2(phen)_2$)], are linked by four $(BPT)^{3-}$ ligands to generate a rhombus, and the neighboring rhombi are linked by carboxylate groups of $(BPT)^{3-}$ to form a unique, independent, 1-D coordination nanotube with a fascinating 1-D → 2-D interdigitated architecture and a 3-D supramolecular network *via* π–π stacking interactions [11]. Wang and coworkers reported $\{[Cd_2(ADC)_2(bpp)_3(H_2O)]_2 \cdot 8H_2O\}_n$ (H_2ADC = 1,3-adamantanedicarboxylic acid,

bpp = 1,3-bis(4-pyridyl)propane), in which $[Cd_4(ADC)_4]$ squares are infinitely connected by bridging bpp ligands to form a 1-D MONT with a mesohelical structure and 1-D → 2-D interdigitated architecture [12]. Wang and coworkers synthesized $[Ni_2(oba)_2(bpy)_2(H_2O)_2]\cdot bpy$ (H_2oba = 4,4′-oxybis(benzoic acid)), in which $[\{Ni(bpy)\}_4]^{8+}$ squares are joined by oba^{2-} bridges to give 1-D nanotubes showing the first example of a polycatenated array of 1-D nanotubes and a 1-D → 2-D polycatenated network [13]. All these structures are different from that of **1** by virtue of the number of ligands joining the metallocycles of the MONT. MONTs that are similar to **1** in the number of linkages between the metallocycles include $[Cu(SCN)(bpp)]\cdot(DMF)_{0.5}$ synthesized by Du and coworkers in which $[Cu_2(bpp)_2]$ metallamacrocycles are linked by two SCN^- bridges [14] and $\{[Zn(btp)(I\text{-}1,3\text{-}bdc)]\cdot 2H_2O\}_n$ (I-1,3-H_2bdc = 5-iodoisophthalic acid) synthesized by Zhang and coworkers in which $[Zn_2(btp)_2]$ rings are linked by two $(I\text{-}1,3\text{-}bdc)^{2-}$ ligands [15].

Because each independent, 1-D MONT in **1** has large voids, corresponding to the 10.27 Å distance between two adjacent $[Mn_2(bte)_2]$ rings, the nitro groups are able to interpenetrate into two adjacent MONTs to form a (1-D → 2-D) interdigitated array. There are weak C–H···O hydrogen bond interactions between H of triazole rings and nitro O ($C(3)\cdots O(5)^{iii}$ (iii, $-x+1$, $y+1$, $-z+1/2$), 3.363(6) Å; $C(5)\cdots O(6)^{iv}$ (iv, $-x+1$, y, $-z+1/2$), 3.257(5) Å) (table 3) which may be the thermodynamical driving force for the penetration of the nitro groups into these voids.

There are also hydrogen bond interactions between coordinated water and the chelating carboxylate $(O(7)\cdots O(3)^{i}$ (i, $-x+1$, $-y$, $-z$), 2.689(3) Å) of the adjacent 2-D layers, resulting in a 3-D hydrogen bond architecture [figure 1(c)]. The lattice waters are limited to the cavities of the nanotubes. There are also hydrogen bond interactions between coordinate water and lattice water (O(7)···O(8), 2.764(4) Å), the lattice water and the monodentate

Table 3. Hydrogen bonding parameters for **1**, **2,** and **3**.

D–H···A	d(D–H) (Å)	d(H···A) (Å)	D(D···A) (Å)	∠(DHA) (°)
1				
O(7)–H(1W)···O(8)	0.848(19)	1.93(2)	2.764(4)	167(4)
$O(7)\text{–}H(2W)\cdots O(3)^{i}$	0.848(19)	1.85(2)	2.689(3)	169(4)
$O(8)\text{–}H(3W)\cdots N(2)^{ii}$	0.844(19)	2.30(3)	3.103(4)	160(5)
$O(8)\text{–}H(4W)\cdots O(2)^{i}$	0.846(19)	1.95(2)	2.780(4)	166(5)
$C(3)\text{–}H(3A)\cdots O(5)^{iii}$	0.93	3.01	3.363(6)	104.2
$C(5)\text{–}H(5A)\cdots O(6)^{iv}$	0.93	2.96	3.257(5)	100.3
2				
$O(7)\text{–}H(1W)\cdots O(9)^{i}$	0.77(4)	2.09(4)	2.832(5)	160(4)
$O(7)\text{–}H(2W)\cdots O(2)^{ii}$	0.838(19)	1.85(2)	2.680(4)	172(5)
$O(8)\text{–}H(3W)\cdots O(9)^{iii}$	0.840(19)	2.29(3)	2.912(7)	131(4)
O(8)–H(4W)···O(5)	0.852(19)	2.29(3)	3.024(5)	144(5)
$O(9)\text{–}H(5W)\cdots O(4)^{iv}$	0.84(2)	1.97(2)	2.805(5)	173(6)
O(9)–H(6W)···O(8)	0.849(19)	2.07(3)	2.870(5)	155(4)
3				
$O(7)\text{–}H(1W)\cdots O(2)^{i}$	0.78(4)	1.98(4)	2.752(3)	172(4)
$O(7)\text{–}H(2W)\cdots O(8)^{i}$	0.92(4)	1.81(4)	2.717(3)	168(3)
O(8)–H(3W)···O(3)	0.74(4)	2.11(4)	2.823(3)	162(4)
$O(8)\text{–}H(4W)\cdots N(2)^{ii}$	0.91(5)	2.09(5)	2.983(3)	166(4)
$C(5)\text{–}H(5A)\cdots O(5)^{iii}$	0.93	3.07	3.349(3)	99.1

Symmetry transformations used to generate equivalent atoms: for **1**, i, $-x+1$, $-y$, $-z$; ii, $x+1/2$, $y-1/2$, z; iii, $-x+1$, $y+1$, $-z+1/2$; iv, $-x+1$, y, $-z+1/2$; for **2**, i, $-x-1$, $-y+1$, $-z+2$; ii, $-x$, $-y+1$, $-z+1$; iii, $-x-1$, $-y$, $-z+3$; iv, $x-1$, y, $z+1$; for **3**, i, $-x+1/2$, $y-1/2$, $-z+1/2$; ii, $-x+3/2$, $y+1/2$, $-z+1/2$; iii, $-x+1$, $-y+2$, $-z$.

carboxylate group (O(8)···O(2)^{i}, 2.780(4) Å), and the lattice water and the non-coordinated 2-N of the triazole ring (O(8)···N(2)^{ii} (ii, $x+1/2$, $y-1/2$, z), 3.103(4) Å) (table 3). These hydrogen bond interactions further stabilize the 3-D architecture in **1**.

The structure of **2** is an undulating 2-D (4,4) network. The asymmetric unit consists of one Mn(II), one $(NO_2\text{-}1,3\text{-bdc})^{2-}$, one btp, one coordinated water, and two lattice waters. Each Mn(II) displays a distorted octahedral coordination geometry, coordinated by three oxygens from two $(NO_2\text{-}1,3\text{-bdc})^{2-}$ ligands (Mn(1)–O(1), 2.267(3) Å; Mn(1)–O(2), 2.385 (2) Å; Mn(1)–O(3A), 2.117(3) Å), the coordinated water (Mn(1)–O(7), 2.177(3) Å), and two nitrogens from two btp ligands (Mn(1)–N(3), 2.240(3) Å; Mn(1)–N(6B), 2.219(3) Å) [figure 2(a)]. The Mn–O and Mn–N bond lengths are similar to those in **1**. Each $(NO_2\text{-}1,3\text{-bdc})^{2-}$ also adopts monodentate and bidentate chelating modes, as in **1**. Each Mn(II) node of the 2-D network is surrounded by four other Mn(II) nodes that are bridged by btp and $(NO_2\text{-}1,3\text{-bdc})^{2-}$ ligands [figure 2(b)]. The btp exhibits an *anti–anti* conformation with a dihedral angle between two triazole planes of 63.4(2)°. Four Mn(II) ions, two btp ligands, and two $(NO_2\text{-}1,3\text{-bdc})^{2-}$ ligands form a $[Mn_4(btp)_2(NO_2\text{-}1,3\text{-bdc})_2]$ unit with Mn···Mn distances of 11.051(3) and 10.2447(13) Å between the btp and $(NO_2\text{-}1,3\text{-bdc})^{2-}$ ligands, respectively.

Intersheet hydrogen bond interactions between coordinated water and carboxylate of $(NO_2\text{-}1,3\text{-bdc})^{2-}$ anions (O7···O2^{ii} (ii, −x, −y + 1, −z + 1), 2.680(4) Å) sustain the interpenetrating double-layer network in **2** [figure 2(c)]. The hydrogen bond interactions between coordinated water and lattice water and between lattice water and carboxylate and nitro construct a 3-D hydrogen bond network (table 3).

Compound **3** exhibits an independent, 1-D MONT based on helical chain subunits. The asymmetric unit contains one Mn(II), one $(NO_2\text{-}1,3\text{-bdc})^{2-}$, one btb, one coordinated water, and one lattice water. Each Mn(II) displays a distorted, $\{MnN_2O_4\}$ octahedral coordination geometry, from two triazole nitrogens from two bte ligands (Mn(1)–N(3), 2.267(2) Å; Mn (1)–N(6A), 2.204(2) Å), three carboxylate oxygens from two $(NO_2\text{-}1,3\text{-bdc})^{2-}$ anions (Mn (1)–O(1) 2.1091(16) Å; Mn(1)–O(3B), 2.3343(16) Å; Mn(1)–O(4B), 2.2744(16) Å), and one coordinated water (Mn(1)–O(7), 2.1912(19) Å) [figure 3(a)], all of which are very similar to the corresponding bond lengths in **1** and **2**. Each btb ligand has an *anti–anti-gauche* conformation with dihedral angles of 121.4(2)° between the two triazole rings and 53.4(4) and 87.9(4)° between the triazole rings and C1–C4 plane. The N1–C1–C2–C3, C1–C2–C3–C4, and C2–C3–C4–N4 torsion angles are 159.0(2)°, 165.1(2)°, and 55.4(3)°, respectively. Each btb is bis-monodentate and bridges two Mn(II) ions with a Mn···Mn separation of 9.975(2) Å.

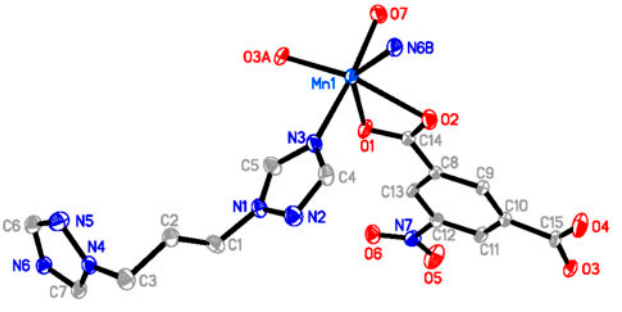

Figure 2(a). The coordination environment of Mn(II) in **2** shown with 50% probability thermal ellipsoids.

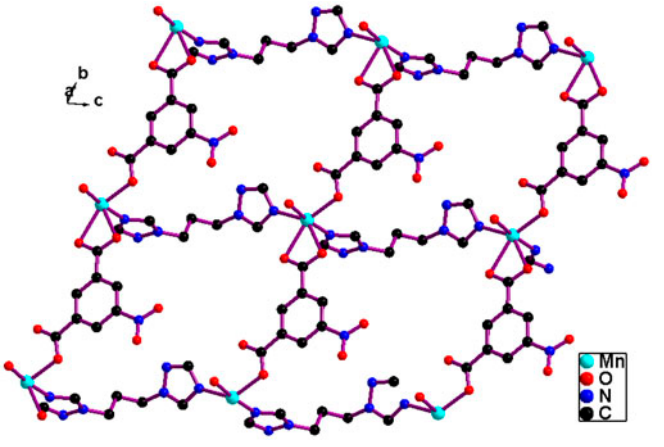

Figure 2(b). The 2-D (4,4) network in **2**.

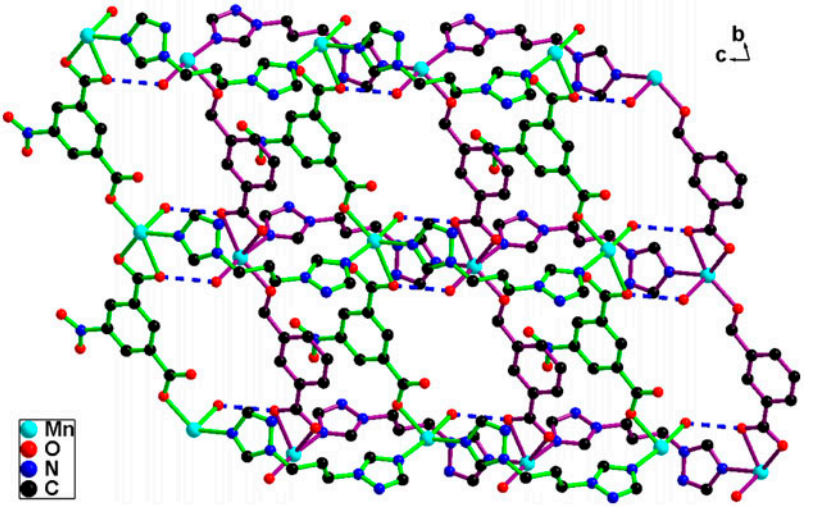

Figure 2(c). Double layer construction in **2** sustained by O–H···O hydrogen bond interactions. The blue dashed lines show the O7···O2^{ii} hydrogen bond interaction.

One interesting structural feature of **3** is that each btb links two Mn(II) ions and extends to form a single, right- or left-handed $[Mn(btb)]_n$ helical chain parallel to the *b*-axis. The helices are based on repeating [Mn–btb–Mn–btb–Mn] units, and the helical pitch corresponds to the *b*-axis translation (10.2604(15) Å). Each $(NO_2\text{-}1,3\text{-}bdc)^{2-}$ in **3** has monodentate and bidentate chelating modes, similar to those in **1** and **2**. Each $(NO_2\text{-}1,3\text{-}bdc)^{2-}$ bridges two Mn(II) ions with a Mn···Mn separation of 10.2604(15) Å, corresponding to the *b*-axis translation, and extends to form two $[Mn(NO_2\text{-}1,3\text{-}bdc)]_n$ linear chains. The single helical chain and two linear chains construct an unusual independent, 1-D MONT [figure 3(b)]. Although Wang

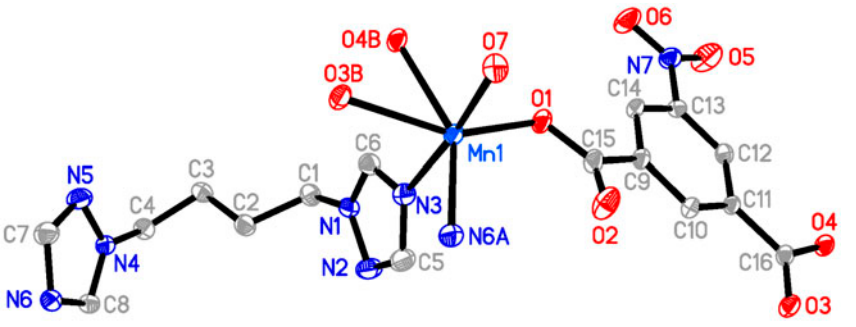

Figure 3(a). The coordination environment of Mn(II) in **3** shown with 50% probability thermal ellipsoids.

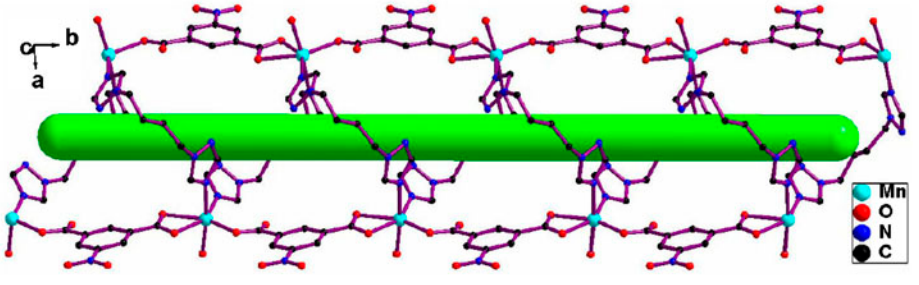

Figure 3(b). Perspective view of an independent, 1-D MONT for **3**.

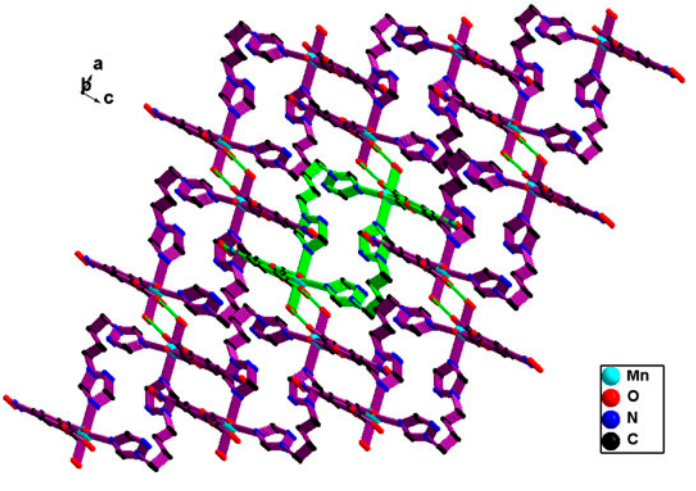

Figure 3(c). The 3-D hydrogen bond architecture in **3**. The bright green dashed lines exhibit the O(7)···O(2)^{i} hydrogen bond interaction.

and coworkers stated that they synthesized the first independent, 1-D MONT with a mesohelical structure [12], **3** is the first independent 1-D MONT constructed by three chains, to the best of our knowledge.

Because each independent, 1-D MONT in **3** has large voids, 10.26 Å long corresponding to the *b*-axis translation, the nitro groups are able to interpenetrate into two adjacent independent 1-D MONTs to form a 1-D → 2-D interdigitated array [figure 3(b)], similar to that of **1**. There are weak C–H···O hydrogen bond interactions between a C–H of the triazole ring and nitro ($C(5)\cdots O(5)^{iii}$ (iii, −x + 1, −y + 2, −z), 3.349(6) Å) (table 3) which may be the thermodynamical driving force for the penetration of the nitro groups into these voids.

There are hydrogen bond interactions between the coordinated water and uncoordinated carboxylate of adjacent 2-D layers ($O(7)\cdots O(2)^{i}$ (i, $-x+1/2$, $y-1/2$, $-z+1/2$), 2.752(3) Å), resulting in a 3-D hydrogen bond supramolecular architecture [figure 3(c)]. The lattice waters are limited to the cavity of the nanotubes. There are also hydrogen bond interactions between coordination water and lattice water ($O(7)\cdots O(8)^{i}$, 2.717(3) Å), and between lattice water and both the chelating carboxylate (O(8)···O(3), 2.823(3) Å) and the uncoordinated 2-N of the triazole ring ($O(8)\cdots N(2)^{ii}$ (ii, $-x+3/2$, $y+1/2$, $-z+1/2$), 2.983(3) Å) (table 3). These hydrogen bond interactions further stabilize the 3-D supramolecular framework in **3**.

1 and **3** show independent, 1-D MONT structures. **2** is an undulating 2-D (4,4) network. Some related Mn(II) coordination polymers are cited as structural comparisons. Liu and coworkers reported $[Mn_2(bcp)_2(bpe)(DMF)]_n$ (H_2bcp = 1,3-bis(4-carboxy-phenoxy)propane and bpe = 1,2-bis(4-pyridyl)ethene), which shows a 2-D → 3-D inclined interpenetration with polyrotaxane character [30]. Zhang and coworkers synthesized $[Mn(tda)(ip)(H_2O)]_n$ [H_2tda = thiophene-2,5-dicarboxylic acid, ip = 1H-imidazo-[4,5-f][1, 10]-phenanthroline], showing a 2-D network and 3-D supramolecular structure through hydrogen bonding and $\pi\cdots\pi$ interactions [31]. Sun and coworkers synthesized [Mn(L)] and [Mn(L)(pybim)] (H_2L = 5-(benzimidazol-1-ylmethyl)isophthalic acid, pybim = 2-(pyridin-2-yl)-1H-benzimidazole) with a uninodal four-connected 2-D network with ($4^4\cdot6^2$) topology and an uninodal three-connected twofold interpenetrated 2-D network with (6^3) topology, respectively [32]. Yan and Li reported $[Mn(dipt)(1,3\text{-}bdc)]_n$ (dipt = 2-(2,4-dichlorophenyl)-1H-imidazo[4,5-f][1, 10]-phenanthroline, 1,3-H_2bdc = isophthalic acid) with a 1-D chain structure [33]. Yang and coworkers synthesized $\{[Mn_3(bpt)_2(bib)_2(H_2O)_2]\cdot(H_2O)_2\}_n$ (H_3bpt = biphenyl-3,4′,5-tricarboxylic acid, bib = 1,4-bis(imidazolyl)benzene), with a 2-D layer [34]. Li and coworkers synthesized the 3-D network structure $[Mn(bpdc)(H_2O)_2]_n$ ($bpdc^{2-}$ = 2,2′-bipyridyl-4,4′-dicarboxylate) [35]. Zhang and coworkers synthesized $\{[Mn(dtb)(bpe)(H_2O)_2]H_2O\}_n$ and $\{[Mn(dtb)(bpa)(H_2O)_2]\cdot H_2O\}_n$ (H_2dtb = 5,5′-dithiobis(2-nitrobenzoic acid), bpa = 1,2-bi(4-pyridyl)ethane) with similar 1-D helical chains and 2-D 4^4 chiral layers, and $\{[Mn(dtb)(phen)]\}_n$, showing a 1-D chain outwardly decorated with phen ligands [36]. Chen and coworkers synthesized a 2-D polymer $[Mn(aip)(phen)]_n$ (H_2aip = 5-aminoisophthalic acid) *via* solvothermal methods [37].

3.2. *PXRD and photoluminescent properties*

The measured and simulated PXRD patterns confirm the phase purity of **1**, **2,** and **3** (figures 4–6). The solid-state luminescence spectra of **1**, **2,** and **3** at room temperature are shown in figure 7. Free bte, btp, btb, and NO_2-1,3-H_2bdc display emission band maxima in the solid state at approximately 390, 410, 414, and 420 nm upon excitation

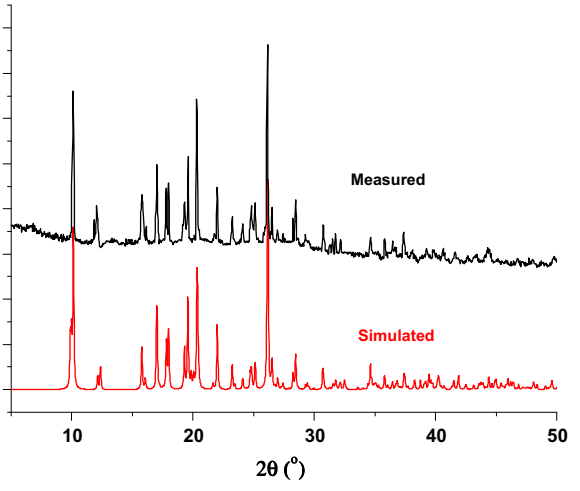

Figure 4. The measured and simulated PXRD patterns for **1**.

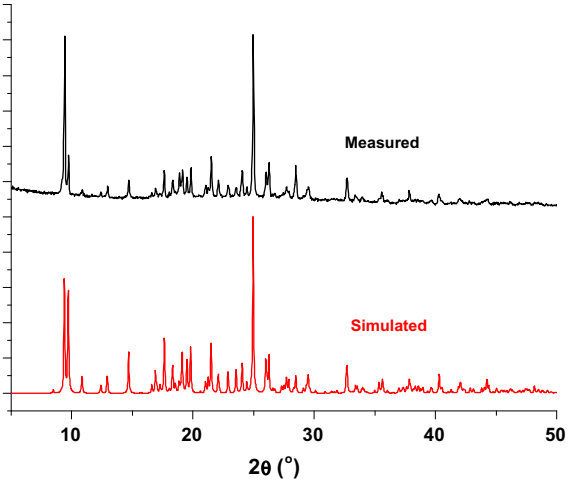

Figure 5. The measured and simulated PXRD patterns for **2**.

at 340 nm. **1** and **3** exhibit blue emission band maxima at approximately 442 and 437 nm, respectively, upon excitation at 340 nm, **2** shows a blue emission band maximum at 414 nm upon excitation at 320 nm. The emission bands can be attributed to ligand-to-metal charge transfer [25–27].

3.3. *Thermal analysis*

To characterize the compounds in terms of thermal stability, the thermal behaviors of **1**, **2,** and **3** were examined by TGA (figure 8). For **1** and **3**, the lattice and coordinated waters were

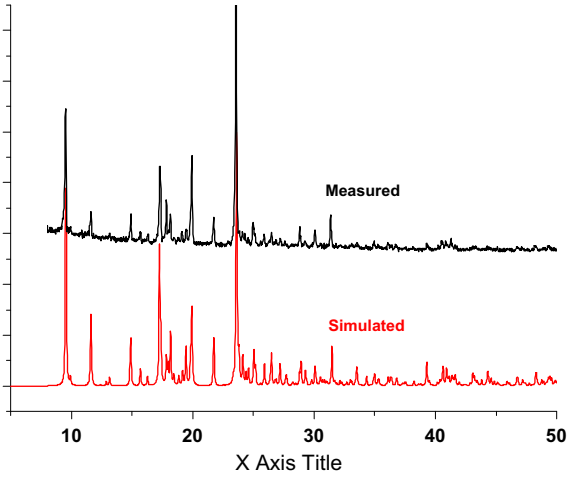

Figure 6. The measured and simulated PXRD patterns for **3**.

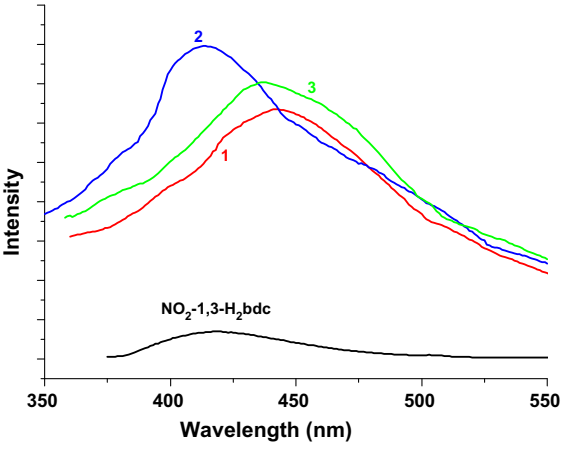

Figure 7. The room temperature, solid state photoluminescent spectra of **1**, **2**, **3** and NO_2-1,3-H_2bdc.

lost from 50 to 148 °C (for **1**, Calcd: 7.76%, found: 7.62%; for **3**, Calcd: 7.32%, found: 7.40%), after which the networks were thermally stable to 200 and 250 °C, respectively. Upon further heating, weight loss occurred continuously and did not stop until 780 °C. The residues at 800 °C are consistent with MnO (for **1**, Calcd: 15.28%, found: 15.46%; for **3**, Calcd: 14.41%, found: 14.62%). For **2**, the lattice and coordinated waters were lost from 50 to 110 °C (Calcd: 10.89%; found: 10.58%), and the network was thermally stable to 280 °C. A rapid weight loss from 315 to 330 °C may be attributed to the loss of one CO_2, one CO, and one NO_2 (Calcd: 23.78%; found: 22.86%). Thereafter, weight loss occurred continuously and did not stop until 780 °C. The residue at 800 °C for **2** is again consistent with MnO (Calcd: 14.29%; found: 14.43%).

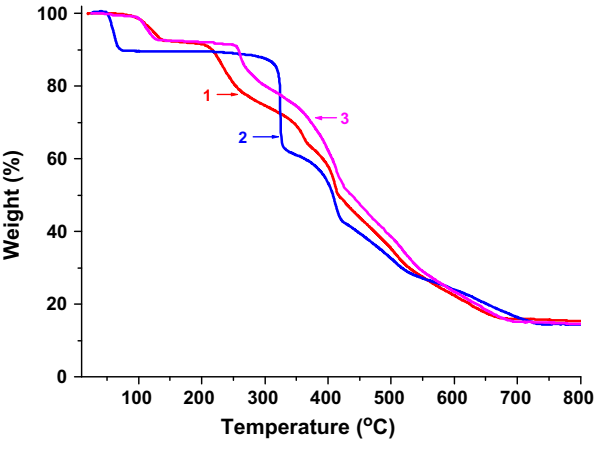

Figure 8. The TG curves of **1**, **2** and **3**.

4. Conclusion

Three Mn(II) coordination polymers were synthesized by combination of the conformationally flexibile ligands bte, btp, btb, with different spacer lengths and the rigid $(NO_2\text{-}1,3\text{-bdc})^{2-}$. **1** is a good example of how two chains connecting ring subunits form an independent, 1-D MONT. **2** is an undulating 2-D (4,4) network. **3** is, to the best of our knowledge, the first independent, 1-D MONT constructed by only three chains. An interesting structural feature of **1** and **3** is that the nitro groups of each independent, 1-D MONT interpenetrate into two adjacent MONTs to form a 1-D → 2-D interdigitated array.

Supplementary material

Crystallographic data for the structural analysis have been deposited with the Cambridge Crystallographic Data Center with CCDC numbers 870610, 870611, and 870612.

Funding

This work was supported by the National Natural Science Foundation of China [grant number 21171126]; the Priority Academic Program Development of Jiangsu Higher Education Institutions, the Funds of Key Laboratory of Organic Synthesis of Jiangsu Province.

References

[1] S. Lijima. *Nature*, **354**, 56 (1991).
[2] R.H. Wang, M.C. Hong, J.H. Luo, R. Cao, J.B. Wang. *Chem. Commun.*, 1018 (2003).
[3] C.Y. Su, A.M. Goforth, M.D. Smith, P.J. Pellechia, H.C. Zur Loye. *J. Am. Chem. Soc.*, **126**, 3576 (2004).
[4] T.T. Luo, H.C. Wu, Y.C. Jao, S.M. Huang, T.W. Tseng, Y.S. Wen, G.H. Lee, S.M. Peng, K.L. Lu. *Angew. Chem. Int. Ed.*, **48**, 9461 (2009).

[5] S. Xiang, J. Huang, L. Li, J. Zhang, L. Jiang, X. Kuang, C.Y. Su. *Inorg. Chem.*, **50**, 1743 (2011).
[6] X.C. Huang, W. Luo, Y.F. Shen, X.J. Lin, D. Li. *Chem. Commun.*, 3995 (2008).
[7] F.N. Dai, H.Y. He, D.F. Sun. *J. Am. Chem. Soc.*, **130**, 14064 (2008).
[8] F.N. Dai, H.Y. He, D.F. Sun. *Inorg. Chem.*, **48**, 4613 (2009).
[9] Y.B. Dong, Y.Y. Jiang, J.P. Ma, F.L. Liu, J. Li, B. Tang, R.Q. Huang, S.R. Batten. *J. Am. Chem. Soc.*, **129**, 4520 (2007).
[10] J. Fan, H.F. Zhu, T. Okamura, W.Y. Sun, W.X. Tang, N. Ueyama. *Inorg. Chem.*, **42**, 158 (2003).
[11] L.N. Li, J.H. Luo, S.Y. Wang, Z.H. Sun, T.L. Chen, M.C. Hong. *Cryst. Growth Des.*, **11**, 3744 (2011).
[12] J.C. Jin, Y.Y. Wang, P. Liu, R.T. Liu, C. Ren, Q.Z. Shi. *Cryst. Growth Des.*, **10**, 2029 (2010).
[13] X.L. Wang, C. Qin, E.B. Wang, Y.G. Li, Z.M. Su, L. Xu, L. Carlucci. *Angew. Chem. Int. Ed.*, **44**, 5824 (2005).
[14] S.B. Ren, X.L. Yang, J. Zhang, Y.Z. Li, Y.X. Zheng, H.B. Du, X.Z. You. *CrystEngComm*, **11**, 246 (2009).
[15] K.L. Zhang, C.T. Hou, J.J. Song, Y. Deng, L. Li, S.W. Ng, G.W. Diao. *CrystEngComm*, **14**, 590 (2012).
[16] N. Chen, M.X. Li, P. Yang, X. He, M. Shao, S.R. Zhu. *Cryst. Growth Des.*, **13**, 2650 (2013).
[17] S. Zhao, Y. Yang, Z. Yang, B.L. Li, Y. Zhang. *J. Coord. Chem.*, **66**, 789 (2013).
[18] H.P. Wang, X.G. Liu, X. Zhu, B.L. Li, B. Wu. *J. Coord. Chem.*, **64**, 4254 (2011).
[19] L.M. Zhu, H.L. Wang, D.Y. Yuan, B.L. Li, H.Y. Li. *J. Coord. Chem.*, **63**, 2307 (2010).
[20] X. Zhu, Q. Chen, Z. Yang, B.L. Li, H.Y. Li. *CrystEngComm*, **15**, 471 (2013).
[21] J. Wang, X. Zhu, Y.F. Cui, B.L. Li, H.Y. Li. *CrystEngComm*, **13**, 3342 (2011).
[22] X. Zhu, L.Y. Wang, X.G. Liu, J. Wang, B.L. Li, H.Y. Li. *CrystEngComm*, **13**, 6090 (2011).
[23] J.J. Perry, J.A. Perman, M.J. Zaworotko. *Chem. Soc. Rev.*, **38**, 1400 (2009).
[24] X. Zhu, J.W. Zhao, B.L. Li, Y. Song, Y.M. Zhang, Y. Zhang. *Inorg. Chem.*, **49**, 1266 (2010).
[25] M. Du, Z.H. Zhang, Y.P. You, X.J. Zhao. *CrystEngComm*, **10**, 306 (2008).
[26] X.Y. Lu, J.W. Ye, W. Li, W.T. Gong, L.J. Yang, Y. Lin, G.L. Ning. *CrystEngComm*, **14**, 1337 (2012).
[27] X. Zhu, P.P. Sun, J.G. Ding, B.L. Li, H.Y. Li. *Cryst. Growth Des.*, **12**, 3992 (2012).
[28] J. Torres, J.L. Lavandera, P. Cabildo, R.M. Claramunt, J. Elguero. *J. Heterocycl. Chem*, **25**, 771 (1988).
[29] G.M. Sheldrick. *Acta Crystallogr., Sect. A: Found Crystallogr.*, **64**, 112 (2008).
[30] J.Q. Liu, J. Wu, Y.Y. Wang, D.Y. Ma. *J. Coord. Chem.*, **65**, 1303 (2012).
[31] X.L. Zhang, K. Cheng. *J. Coord. Chem.*, **65**, 3019 (2012).
[32] H.W. Kuai, T.A. Okamura, W.Y. Sun. *J. Coord. Chem.*, **65**, 3147 (2012).
[33] L. Yan, C.B. Li. *J. Coord. Chem.*, **65**, 4288 (2012).
[34] Y.L. Lu, W.J. Zhao, X. Feng, Y. Chai, Z. Wu, X.W. Yang. *J. Coord. Chem.*, **66**, 473 (2013).
[35] Z.Q. Zhang, J. Li, R.P. Liu, W.X. Zhou, F.X. Zhang. *J. Coord. Chem.*, **66**, 926 (2013).
[36] Y.N. Zhang, Z. Dong, X. Hai, L. Cui, Y.Y. Wang. *J. Coord. Chem.*, **66**, 1676 (2013).
[37] J.J. Wang, Q.L. Bao, J.X. Chen. *J. Coord. Chem.*, **66**, 2578 (2013).